Transition Modelling for Rotorcraft CFD

Georgios Zografakis, George Barakos and Mark Johnson

Department of Engineering, University of Liverpool,
Brownlow Hill, Liverpool L69 3GH, United Kingdom
e-mail: g.zografakis@liverpool.ac.uk
e-mail: g.barakos@liverpool.ac.uk

Key words: laminar to turbulent transition, CFD

Abstract. This paper presents an investigation in the use of transition models for rotorcraft CFD. Simple models for transition prediction based on correlations were first investigated and the results revealed sensitivity of the predictions in the path selected for the integration of boundary layer quantities as well as in the parameters of the correlation. For complex flows like flows around rotors of helicopter fuselages, these models were difficult to implement, parallerise and use. Investigations of more modern closures based on transport equations were not free from problems either. The employed source terms of these models still depend on empirical correlations which have to be carefully evaluated and assessed against CFD and experimental data. The present results suggest that a re-calibration process using detailed measurements of transitional boundary layers may lead to better correlations suitable for the analysis of rotorcraft flows.

NOMENCLATURE:

arc	curvilinear length
C_f	skin friction coefficient, $\tau/\rho U_\infty^2$
C_p	surface pressure coefficient
k	turbulent kinetic energy
K	Flow acceleration parameter
Mach	Mach number
Re	Reynolds number, $\rho x U/\mu$
Re_θ	momentum thickness Reynolds number, $\rho\theta U/\mu$
$Re_{\theta c}$	Critical momentum thickness Reynolds number
$Re_{\theta t}$	Transition momentum thickness Reynolds number, $\rho\theta_t U/\mu$
Re_x	Reynolds number based on the distance from stagnation point, $\rho \cdot arc \cdot U/\mu$
R_v	vorticity Reynolds number
R_T	viscosity ratio
S	absolute value of strain rate, $(2S_{ij}S_{ij})^{1/2}$
S_{ij}	strain rate tensor, $0.5(\partial u_i/\partial x_j - \partial u_j/\partial x_i)$
T	time scale
Tu	turbulence intensity, $100\,(2k/3)^{1/2}/U_\infty$
U	local velocity
U_e	boundary layer edge velocity
U_∞	free-stream velocity

Greek letters

α	incidence angle

β_0 rotor coning
γ intermittency factor
δ boundary layer thickness
θ momentum thickness
θ_0 rotor collective
λ_θ pressure gradient parameter, $(\theta^2/\nu)(du/ds)$
μ molecular viscosity
μ_t eddy viscosity
N_{crit} critical factor for e^N method
ν kinematic viscosity, μ/ρ
ρ density
ω specific turbulence dissipation rate
Ω absolute value of vorticity, $(2\Omega_{ij}\Omega_{ij})^{1/2}$
Ω_{ij} vorticity vector, $0.5(\partial u_i/\partial x_j - \partial u_j/\partial x_i)$

Subscripts

start start of the transition region
end end of the transition region
tr transition point

1. INTRODUCTION

In recent years, Computational Fluid Dynamics has emerged as a tool suitable for the aerodynamic analysis of flows pertinent to rotorcraft applications. Complex flows around rotors or even complete helicopter configurations [1, 2] appear in the literature and comparisons with flight or tunnel test data are encouraging [3]. Still, several problems exist regarding the fidelity of these computations. For example, prediction of rotor power in hover, or accurate prediction of the rotor performance in forward flight is still not routine. Part of the problem is due to the relatively crude turbulence and transition modelling used in many of the current CFD applications. Popular turbulence models in the rotorcraft community still include simple algebraic closures like the Baldwin-Lomax model [4] though some applications of one- and two-equation closures also appear. Most of the time, the employed turbulence models are used with fixed transition positions on the rotor and fuselage or, even worst, free-transition is employed in some investigations. This approach may result in incorrect predictions of boundary layer properties with consequences in the accuracy of the results in terms of drag, separation onset and stall. In this paper, an effort is made to investigate the performance of coupled turbulence and transition modelling approaches within the framework of rotorcraft CFD.

Several transition prediction models are assessed for a range of test cases, in conjunction with the popular k-ω model of Wilcox [5]. The models are assessed not only in terms of their performance but also in terms of their implementation requirements. Early transition models based on simple correlations were first investigated starting from the criterion of Michel [6] and the well-known Cebeci and Smith [7] model.

Very early in this study it was evident that suitable experimental data for assessing the performance of these models were not available for any single case studied in experiments and for this reason a range of test cases were considered. These include the well-known UH60A rotor in forward flight [1], the flow around the ROBIN body [2] as well as flows around aerofoils [8, 9]. The detail of the available experimental data is, for the cases considered here, inversely proportional to the complexity of the cases. Although flows around

helicopter rotors could be closer to a realistic flow configuration, the measured data for such cases include loads and perhaps surface pressure data which may not be suitable for the calibration or the performance assessment of transition models. On the other hand, flows around aerofoils may contain substantial amounts of detailed measurements but the flow configuration may lack some of the essential flow features encountered in full 3D rotor flows.

2. THE HELICOPTER MULTI-BLOCK SOLVER

The Helicopter Multi-Block solver of Liverpool (HMB) is the main CFD tool employed for this work and the framework for assessing several transition prediction models. This code offers a range of turbulence models and is suitable for the analysis of complex flows due to its unique features which include sliding grids, blade actuation and rotor trimming as well as an efficient algorithm for solving the Navier-Stokes equations along with transport equations of one- and two-equation turbulence models. The details of the solver are described elsewhere and here only an outline is presented.

The unsteady Navier-Stokes equations are discretised on a curvilinear multi-block body conforming mesh using a cell-centred finite volume method. The convective terms are discretised using Osher's upwind scheme. MUSCL variable extrapolation is used to provide second-order accuracy with the Van Albada limiter. A central discretisation method is used for the viscous terms. The solver includes a range of one- and two-equation turbulence models and a Smagorinsky LES and Spalart-Almaras DES model. A dual-time stepping method is employed for time-accurate simulations, where the time derivative is approximated by a second-order backward difference [10]. The resulting nonlinear system of equations is solved by integration in pseudo-time using a first-order backward difference. In each pseudo-time step, a linearisation is used to obtain a system of equations, which is solved using a Generalised Conjugate Gradient method with a Block Incomplete Lower-Upper (BILU) pre-conditioner.

To obtain an efficient parallel method based on domain decomposition, the method should have a good serial performance when applied to the domains allocated to the different processes, combined with a minimal communication. To achieve this aim, the flow solver uses the following methods:

- The flux Jacobians resulting from the linearisation in pseudo-time are employed in an approximate form that reduces the number of non-zero entries and as a result the size of the linear system. The use of the approximate Jacobian also reduces the parallel communication since only one row of halo cells is needed by the neighbouring process in the linear solver instead of two in the case of an 'exact' Jacobian.
- The communication between processes is minimised by decoupling the BILU factorization between blocks.
- On each processor a vector is allocated that contains all the halo cells for all grid blocks.
- Inter-process communication is performed by sending a series of messages between the respective processes, each corresponding to a block connection, containing the halo cell data. The messages are sent in chunks of 10,000 double precision numbers using non-blocking send and receive MPI function.

This method has been used on a range of platforms, including Beowulf clusters consisting of various generations of Pentium processors and multi-processor workstations. Recently, the solver was ported to the HPCx computer at Daresbury Laboratory. The HPCx system comprises 50 IBM Power4+ Regatta nodes, i.e. 1600 processors, delivering a peak performance of 10.8 TeraFlops.

Further details regarding this solver as well as validation of the method can be found in references [1-2,10-11].

The governing equations are the Reynolds-averaged Navier-Stokes equations and the turbulence model employed is the two equation k-ω turbulence model described by Wilcox [5].

3. TRANSITION MODELS

Low Reynolds number eddy-viscosity turbulent models have the ability to predict transition. Unfortunately, comparison with experiments shows that they give unsatisfactory early the transition onsets. This shows the need for another way of correct estimation of transition. These approaches include simple correlation models like Michel's criterion [6] or the Cebeci-Smith method[7] as well as transition models based on the solution of transport equations.
Michel's criterion [6] is a simple model based on experimental data. It correlates the local values of momentum thickness with the position of the transition point. This criterion assumes that the onset of transitional flow occurs when the Reynolds number based on the momentum thickness exceeds a specific value of

$$\mathrm{Re}_{\theta,tr} \approx \frac{U(x)\theta(x)}{\nu} \approx 2.9\mathrm{Re}_{x,tr}^{0.4} \tag{1}$$

where $\mathrm{Re}_{x,tr}$ is the Reynolds number, based on the distance measured from the stagnation point.
The second empirical correlation employed here is the Cebeci-Smith model [7]. This model also correlates the momentum thickness Reynolds number with the local transition Reynolds number and states that:

$$\mathrm{Re}_{\theta,tr} = 1.174(1+\frac{22400}{\mathrm{Re}_{x,tr}})\mathrm{Re}_{x,tr}^{0.46} \tag{2}$$

Both criteria require integration of boundary layer parameters. The estimation of the momentum thickness Reynolds number requires the calculation of boundary layer momentum thickness. This is achieved by Thwaite's' method [12] which relates the momentum thickness of the boundary layer with the integration of the velocity at the edge of it,

$$\theta^2 \approx \frac{0.45\nu}{U_e^6}\int_{x_0}^{x} U_e^5 dx \tag{3}$$

where u_e is the velocity at the edge of the boundary layer and is can be given as a function of pressure distribution,

$$u_e = U_\infty\sqrt{1-C_p} \tag{4}$$

Menter *et al.*[13] developed a model based on transport built on local variables. Two transport equations are used in this model. The first one is for the intermittency γ and triggers the transition locally. The second transport equation is solved in term of the transition onset momentum thickness Reynolds number ($\mathrm{Re}_{\theta,tr}$) and it is used to restrict the dependence of the model only on local variables.
The transport equation for the intermittency factor (γ) reads

$$\frac{\partial(\rho\gamma)}{\partial t}+\frac{\partial(\rho u_j\gamma)}{\partial x_j} = P_{\gamma 1}-E_{\gamma 1}+P_{\gamma 2}-E_{\gamma 1}+\frac{\partial}{\partial x_j}[(\mu+\frac{\mu_t}{\sigma_f})\frac{\partial\gamma}{\partial x_j}] \tag{5}$$

where the terms $P_{\gamma 1}, P_{\gamma 2}$ and $E_{\gamma 1}, E_{\gamma 1}$ are the production and dissipation terms respectively of the equation and are functions of the vorticity Reynolds number and the critical momentum thickness Reynolds number,

$$P_{\gamma 1} = F_{length} C_{\alpha 1} \rho S (\gamma F_{onset})^{c_\alpha} \tag{6}$$

$$P_{\gamma 2} = C_{\alpha 2} \rho \Omega \gamma F_{turb} \tag{7}$$

$$E_{\gamma 1} = C_{e1} P_{\gamma 1} \gamma \tag{8}$$

$$E2 = C_{e2} P_{\gamma 2} \gamma \tag{9}$$

where Ω is the vorticity magnitude, S is the strain rate magnitude and, F_{length} is an empirical correlation that controls the length of the transition region. The function F_{onset} which controls the production $P_{\gamma 1}$ is estimated from the following equations:

$$F_{onset} = \max[F_{onset2} - F_{onset3}, 0] \tag{10}$$

$$F_{onset3} = \max[1 - (\mathrm{Re}_T / 2.5)^3, 0] \tag{11}$$

$$F_{onset2} = \min[max[F_{onset1}, F_{onset1}^4, 2.0] \tag{12}$$

$$F_{onset1} = \frac{\mathrm{Re}_v}{2.193 \mathrm{Re}_{\theta c}} \tag{13}$$

$$F_{turb} = e^{[-(\mathrm{Re}_T / 4)^4]} \tag{14}$$

where the vorticity Reynolds number Re_v and the viscosity ratio R_T are given by the following equations :

$$\mathrm{Re}_v = \frac{\rho S y^2}{\mu} \text{ and } \mathrm{R}_T = \frac{\rho k}{\mu \omega}. \tag{15}$$

$\mathrm{Re}_{\theta c}$ is the critical momentum thickness Reynolds number, ω is the specific turbulence dissipation rate and k is the turbulence kinetic energy.

The transition onset momentum thickness Reynolds number is given by:

$$\frac{\partial(\rho \tilde{\mathrm{Re}}_{\theta t})}{\partial t} + \frac{\partial(\rho u_j \tilde{\mathrm{Re}}_{\theta t})}{\partial x_j} = P_{\theta t} + \frac{\partial}{\partial x_j}[\sigma_{\theta t}(\mu + \mu_t)\frac{\partial \tilde{\mathrm{Re}}_{\theta t}}{\partial x_j}] \tag{16}$$

The source term $P_{\theta t}$ is defined as follows:

$$P_{\theta t} = C_{\theta t}(\frac{\rho}{T})(\mathrm{Re}_{\theta t} - \tilde{\mathrm{Re}}_{\theta t})(1.0 - F_{\theta t}) \tag{17}$$

where $\tilde{\mathrm{Re}}_{\theta,tr}$ is the scalar momentum thickness Reynolds number, T is the time scale for dimensional reasons and $F_{\theta,tr}$ is a blending function for turning off the influence of the production term $P_{\theta t}$ inside the boundary layer.

The previous functions are given by:

$$T = \frac{500\mu}{\rho U^2} \tag{18}$$

$$F_{\theta t} = \min[\max[F_{wake} e^{-(y/\delta)^4}, 1.0 - (\frac{C_{e2}\gamma - 1}{C_{e2} - 1}), 1.0] \tag{19}$$

$$F_{wake} = e^{[-(\mathrm{Re}_\omega / 10^5)^2]}, \ \mathrm{Re}_v = \frac{\rho \omega y^2}{\mu} \tag{20}$$

$$\delta = \frac{50\Omega y}{U}\delta_{BL},\ \ \delta_{BL} = \frac{15\theta_{BL}}{2},\ \ \theta_{BL} = \frac{\mathrm{Re}_{\theta t}\mu}{\rho U} \tag{21}$$

where U is the local velocity magnitude and the model constants are $C_{\alpha 1} = 2.0$, $C_{e1} = 1.0$, $C_{\alpha 2} = 0.06$, $C_{e2} = 50.0$, $C_{\alpha} = 0.5$, $C_{\theta t} = 0.03$ and $\sigma_{\gamma} = 1.0$, $\sigma_{\theta t} = 2.0$.

The model is coupled with the SST turbulence model as follows:

$$\tilde{P}_k = \gamma_{eff} P_k \tag{22}$$

$$\tilde{D}_k = \min[max[\gamma_{eff}, 0.1], 1.0] D_k \tag{23}$$

where the terms P_k and D_k are the production and destruction terms of the turbulent kinetic energy equation in the original SST turbulence model. The factor γ_{eff} is given by the following equations:

$$\gamma_{eff} = \max[\gamma_{sep}, \gamma] \tag{24}$$

The factor γ_{sep} is derived from the modification of the transition model for the case where separation of the laminar boundary layer occurs. This modification allows the intermittency to obtain values higher than one in order the flow to reattach. The equation for the γ_{sep} is given below:

$$\gamma_{sep} = \min[0.8 max[F_{onset1} - 1.0, 0] F_{reattach}, 5.0] F_{\theta t} \tag{25}$$

$$F_{reattach} = e^{[-(\mathrm{Re}_T/15)^4]} \tag{26}$$

For the calculation of the proprietary functions of the transition model, a set of correlations were introduced. This set of empirical correlations is derived from the work of the Misaka and Obayashi [14]. For the transition onset Reynolds number in the flow field, the correlation was defined as:

$$\mathrm{Re}_{\theta t} = \left[110.0 + e^{(7.08 + Tu)}\right] F(\lambda_{\theta}, K) \tag{27}$$

For the correlation of the $\mathrm{Re}_{\theta c}$, the following has been suggested:

$$\mathrm{Re}_{\theta c} = 0.9\tilde{\mathrm{Re}}_{\theta t} \tag{28}$$

The function F_{length} was derived from a Mayle's definition [15] and is given as

$$F_{lenght} = 1260\tilde{\mathrm{Re}}_{\theta t}\frac{\mu}{\rho U}\frac{1}{\mathrm{Re}} \tag{29}$$

For the calculation of the end of transition, the correlation of Abu-Ghannam and Shaw [16] was used. The end of the transition is estimated as a function of the length Reynolds number $\mathrm{Re}_{x,start}$ at the start of transition and is given by:

$$\mathrm{Re}_{x,end} = \mathrm{Re}_{x,start} + 16.8(\mathrm{Re}_{x,start})^{0.5} \tag{30}$$

4. TEST CASES

For the validation of the methods a number of test cases has been selected which includes flows around aerofoils, rotors and helicopter fuselage bodies.

In the present work, two aerofoils were used. The first one is the NACA 0012 aerofoil for which computations were performed under two different conditions. Initially, the aerofoil was tested at Mach number of 0.4 and at Reynolds number of 2.88×10^6. Another set of conditions was considered for the NACA 0012 at a lower Reynolds number of 10^5 and at

Mach number of M=0.2. All the computations were compared with the experimental results from the LABM laboratory [8].
As a second aerofoil, the ONERA A-Aerofoil was selected which was the focus for a European research project [9]. Several flow parameters were measured, including surface pressure coefficient, skin friction and a detailed boundary layer velocity profiles. The flow around ONERA A-Aerofoil was selected due to the challenges it poses for all turbulence models: high pressure gradients, near stall flow and high surface curvature.
The computations for the ONERA A-Aerofoil were performed for constant Mach number of 0.15 and for three Reynolds numbers, at $2x10^6$, $3.13x10^6$ and $5.25x10^6$, which were the conditions for the tests in the F1 and F2 wind tunnels of ONERA.
Beside the flow around aerofoils, more complex cases were also considered. These included the flow around the ROBIN fuselage body, calculated at both -5^o and 5^o angle of attack. For the calculations, a Mach number of 0.064 and a Reynolds number of $4.47\ 10^6$ were considered and the transition point was estimated at 5 different slices along the body, three on the fuselage and two on the hub-shroud. The z/R coordinates of each slice are presented in Table 1.

Slice	z/R
1	-0.004426
2	0.002182
3	0.0795
4	0.1415
5	0.1724

Table 1. Slice coordinates of ROBIN fuselage body employed for transition prediction.

Validation for rotor cases has been obtained for the UH-60A rotor in forward flight. The conditions considered here were derived from the U.S. Army/NASA UH-60A Airloads Program[1]. The rotor was tested at advance ratio μ=0.368, and tip Mach number M_{tip}=0.67. Table 2 presents the detailed conditions.

Case	μ	M_{tip}	θ_{shaft}	θ_0	θ_{1s}	θ_{1c}	β_{1c}	β_0	β_{1c}
UH-60A	0.368	0.67	7.3	14.6	8.63	-2.39	3.43	-1.04	-0.7

Table 2. Parameter of the forward-flight case of UH-60A rotor.

5. RESULTS AND DISCUSSION

Results for the transition prediction on the UH60A rotor are presented in Figures 1-9. The planform of the blade with the associated sections and twist is shown in Figure 1, while Figure 2 presents an overview of the complex flow-field around his blade using the Q-criterion. The obtained results for the sectional pitch and moment coefficients at r/R of 0.865 are shown in Figure 3. Good agreement with the experiments can be seen for the advancing side of the rotor, and even on the retreating side results are in fair agreement with measurements. For this case a fine grid has been used and the blade was allowed to deform in twist as described in [1].
The predicted transition points on the upper and lower surfaces of the blade are shown in Figure 4 at two azimuth angles of 60 and 315 degrees. As one moves from the root to the tip of the blade, the transition point moves towards the leading edge on the suction side while the pressure side remains laminar up to about 80% of the chord near the tip. Due to the higher incidence angles encountered on the retreating side of the rotor, the results for 315 degrees of azimuth suggest that the lower side of the blade is laminar while on the suction side transition occurs at about 10% of the chord. The differences between the predictions obtained by the Michel and Cebeci-Smith models are small and the results suggest that the transition point is

mainly dictated by the blade incidence angle. Figure 5 presents the variation of the transition point as a function of the azimuth angle for two stations at r/R=0.85 and 0.95. The results suggest that the transition point moves forward on the retreating side and aft on the advancing side of the rotor. This could be associated with the relatively low incidence angles encountered on the advancing side of the disk and the corresponding reduction of the lift coefficient at these low angles. The results for the outboard station show that at 90 degrees of azimuth, transition occurs earlier on the lower side of the blade. At this station and for 90 degrees of azimuth, the blade may be experiencing negative lift and very low incidence angles and for this reason the lower side of the blade has an earlier transition point. The boundary between laminar and turbulent flow is shown in Figure 6 at several azimuth angles with detailed views for the lower and upper surface at 300 degrees of azimuth presented in Figure 7. Figures 8 and 9 present additional results for azimuth angles of 45, 135, 225 and 315 degrees. Unfortunately, the available experimental data for this case provide little insight in the effects of transition and consequently no further comparisons are possible.

Figure 10 presents a comparison between CFD and experiments for surface pressure distribution on the ROBIN fuselage. The results show good agreement with the measurements for many of the stations along the body. A schematic of the pressure taps over the ROBIN fuselage body can be seen in Figure 10(a). An incidence angle of 5 degrees was selected for this case and the computations were conducted at a Mach number 0.064 and Reynolds number of 4.47 millions, to match the experiments of NASA [3]. Figure 11 presents the transition location predicted with several models at three stations along the z axis. For this test case the predictions of the Michel and Cebeci-Smith models are close while the Abu-Ghannam and Shaw model predicts the transition slightly downstream. The sensitivity of the predictions with the later model is also shown. Results are presented for several values of the correlation parameter of equation 28. The end of the transition is influenced by this parameter and the present set of results suggests that this parameter could be further calibrated based on test data so that the model can give realistic predictions for complex flows. Again, the available data for this test case provide little support for the calibration of the models and strict assessment of their performance. For this reason, aerofoil flows were also considered due the availability of detailed flow measurements.

Figure 12 presents results for the transition location on the upper and lower sides of a NACA0012 aerofoil as a function of incidence. For this test case, results of the HMB solver are also compared against the popular aerofoil code, XFOIL [16] which uses the e^N method for transition prediction. The overall trend of the obtained results is similar for all models and good agreement is obtained with test data from [8] for the suction side of the section. On the pressure side, XFOIL predicted a relatively late transition in comparison to the other models. Further predictions for the onset and end of the transition are shown in Figure 13. One can see that tuning of the correlation parameters can provide better agreement with the test data though results are still not satisfactory.

To quantify the effect of the transition on the predicted sectional loads, the flow around the ONERA A-aerofoil was also computed ($\alpha=7.2^o$, $\alpha=12.3^o$, $\alpha=13.3^o$, Mach number of 0.15 and Reynolds number of $2x10^6$). Figure 14 presents results for the surface pressure coefficient, where the suction peak is better resolved with the employed transition models than with free-transition based on the k-ω model alone. The results show very good agreement for the surface pressure coefficient and for the skin friction at several incidence angles up to near-stall conditions. The skin friction distributions show clearly the transition point and agreement with the available experimental data is good. Very few measurements are, however, available for the flow of near the leading edge of this section. Figure 15 compares the transition point predictions between the employed models. For this section, the

transition point moves relatively less in comparison to the NACA 0012 aerofoil and the employed models agree fairly well for the suction side.

Figure 16 presents results with the k-ω–γ- Re_θ model [13] for the flow around a NACA0012 aerofoil. The flow near the leading edge of the section suggests that a laminar separation bubble is present which is responsible for the onset of transition. The size of this bubble and consequently the realism of the computed results depend on the values of γ and the growth of the turbulent boundary layer downstream. The results of Figure 16 suggest a late transition to turbulence since the flow failed to turn turbulent immediately over the bubble. This observation fuelled a detailed investigation of the flow and the individual terms of the model. The obtained predictions suggest that model depends on the employed correlation of equations 27 and 28. This correlation has to be obtained based on experiments and apparently depends on the flow configuration at hand. The field of equation 27 is shown in Figure 16(c). This function depends on the level of free-stream turbulence (Tu), the local pressure gradient (λ_Θ) and the local flow acceleration parameter K (Figure 16(d)). This function undergoes rapid changes near the leading edge of the section which are reflected in the obtained results. Further investigation revealed that the behaviour of this correlation is mainly influenced by the flow acceleration parameter near the leading edge of the aerofoil (Figures 16(e) and (f)). The exact form of the correlation is not clear and there is no unique definition in the literature. It is, however, possible to obtain such correlation from wind-tunnel measurements.

The obtained results suggest that the employed transition models predict, at least in a qualitative sense, the onset of transition. However, the simple correlation-based models require detailed survey of the flow and a judicious selection of the integration path for estimating the transition onset. Further, calculation of wall-distances and boundary-layer thickness is required which may not easy for complex flows. On the other hand models based on transport equations fit better with the overall computational framework of CFD solvers and are relatively easy to implement. They are not free from empirical correlations though and as suggested by the present results, the predictions of these models depend on correlations between the free-stream turbulence, the flow acceleration and the momentum-thickness Reynolds number. Such correlations are difficult to devise based on intuition alone and require the use of tunnel data for a range of cases.

6. SUMMARY AND FUTURE STEPS

The present work established a basis for assessing the performance of transition prediction models for rotorcraft flows. Several models were assessed in terms of their accuracy and ease of implementation in CFD solvers and results have been obtained for a range of cases from simple flows around aerofoils to flows around rotors and a helicopter fuselage. Models based on transport equations were found to still depend on correlations for their source terms and evaluation of some of these sources depends on the specifics of the flow at hand. Consequently, detailed experimental data are necessary for calibration and improvement of these correlations. Based on the current findings, this work is directed towards an experimental investigation of simple transitional flows in order to build a database which will be use for calibration of transition correlations in conjunction with intermittency-based models.

Acknowledgment.
This project is supported by Westland Helicopters and the University of Liverpool.

REFERENCES

[1] R. Steijl, G. Barakos, and K. Badcock, "*A Framework for CFD Analysis of Rotors in Hover and Forward Flight*", Int. J. for Num. Meth. in Fluids, vol. 51, 2006, pp. 819-847.

[2] G. Barakos, and et. al., "*CFD Capability for Fully Helicopter Engineering Analysis"*, 31st European Rotorcraft Forum, Florence, Italy September 2005.

[3] C. Freeman, and R. Mineck, "*Fuselage Pressure Measurements of a Helicopter Wind tunnel with a 3.15meter Diameter Single Rotor*", NASA Technical Report No.80051, 1979.

[4] B.S. Baldwin, and H. Lomax, "*Thin Layer Approximation and Algebraic Model for Separated Turbulent Flows"*, 16th AIAA Aerospace Sciences Meeting and Exhibit, Huntsville, Alabama, January 1978.

[5] D.C. Wilcox, "*Reassessment of the Scale-Determining Equation for Advanced Turbulence Models*", *AIAA Journal*, vol. 26, 1988, pp. 1299–1310.

[6] R. Michel, "*Etude de la Transition sur les Profils d'Aile, Etablissementd'um Critere de Determination Point de Transition et Calcul de la Trainee de Profil Incompressible*", ONERA, 1951.

[7] T. Cebeci, and A.M.O. Smith, "*Analysis of Turbulent Boundary Layer*", Academic Press*,* 1974.

[8] A. Benyahia, and et al., *"Detailed Evaluation of CFD Predictions Against LDA Measurements for Flow on an Airfoil",* In Integrated CFD and Experiments, Glasgow, UK, September 2003.

[9] W. Haase, E. Chaput, E. Elsholz, M.A. Leschziner, and U.R. Muller, "*ECARP: European Computational Aerodynamics Research Project: Validation of Turbulence Models*", Notes on Numerical Fluid Mechanics, vol 58, 1997.

[10] A. Spentzos, G. Barakos, and Badcock, P. Richards, B.E. Wenert, S. Schreck, and M. Raffel, *"CFD Investigation of 2D and 3D Dynamic Stall",* AIAA Journal, vol 34, no 5, 2005, pp. 1023–1033.

[11] R. Morvant, K. Badcock, G. Barakos, and B.E. Richards, *"Aerofoil-Vortex Interaction Using the Compressible Vorticity Confinement Method",* AIAA Journal, vol 43, no 1, 2004, pp. 63–75.

[12] B. Thwaite, "*Approximate Calculation of the Laminar Boundary Layer"*, Aeronautical Quarterly, 1:245-280, 1949.

[13] F.R. Menter, and et al. "*A Correlation-Based Transition Model Using Local Variables – Part I: Model Formulation*"*,* Journal of Turbomachinery*,* vol. 128, 2006, pp. 423-433.

[14] T. Misaka, and S. Obayashi, "*Application of Local Correlation-Based Transition Model to Flows around Wings"*, In 44*th* AIAA Aerospace Sciences Meeting, vol. 15, pp. 10973–10983, Reno, NV, January 2006.

[15] R.E. Mayle, "*The Role of Laminar-Turbulent Transition in Gas Turbine Engines*", Journal of Turbomachinery, 113:509–537, 1991.

[16] B.J. Abu-Ghannam, and R. Shaw, "*Natural Transition of Boundary Layers – The Effects of Turbulence, Pressure Gradients and Flow History*"*,* Journal of Mechanical Engineering Science*, vol.* 22, no 5, 1980, pp. 213-228.

[17] M. Drela and H. Youngren, XFOIL 6.9 User Guide, 2001.

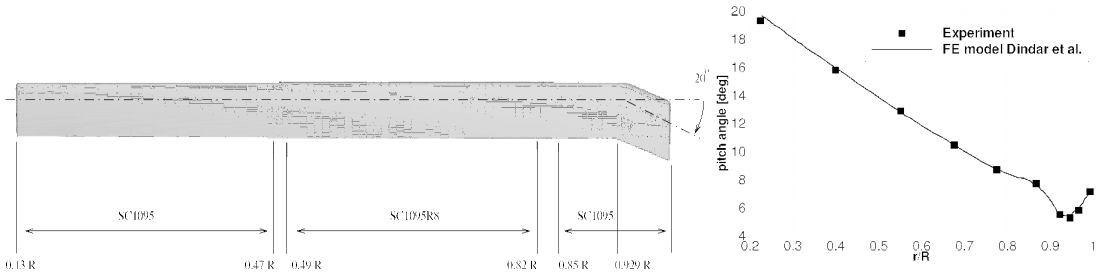

Figure 1: Geometry and twist distribution of the UH-60A rotor blade.

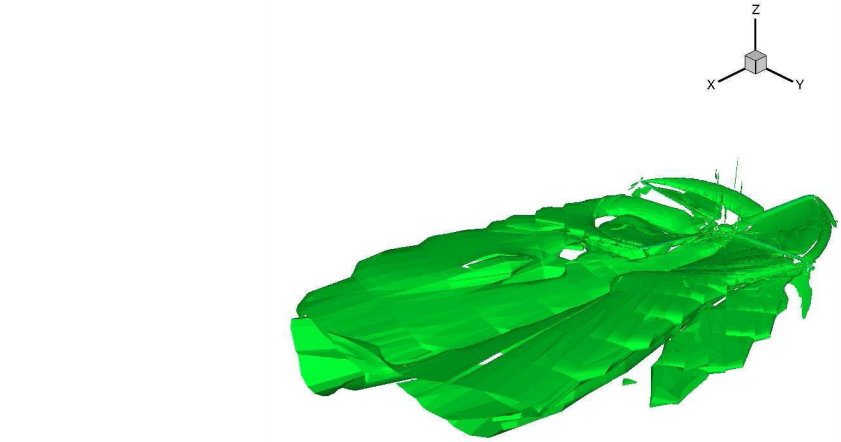

Figure 2: Flow visualization of the fast forward flight for a UH-60A rotor. The fight conditions correspond to an advance ratio at μ=0.368 and tip Mach number at M_{tip}=0.67.

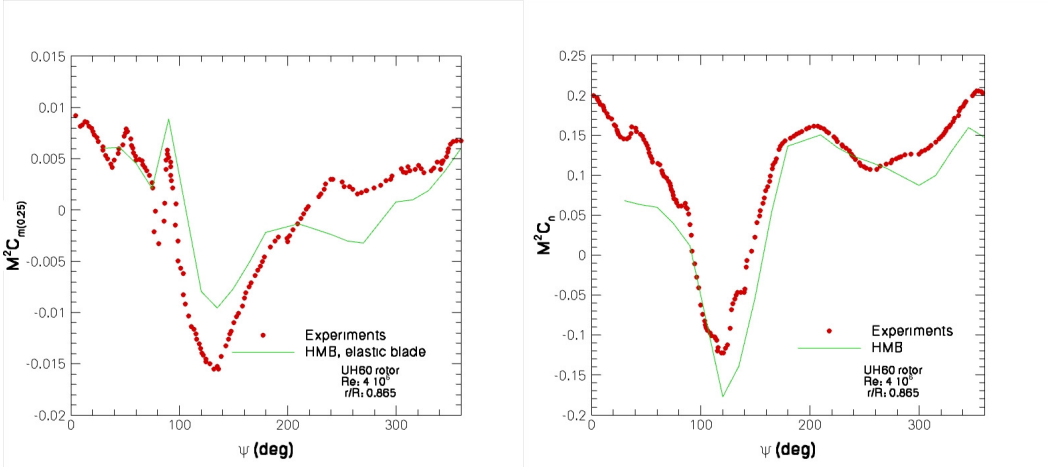

Figure 3: Azimuth variation of the pitching moment and the sectional normal force for the UH-60A rotor. The results are for a fast forward flight and are calculated at r/R=0.865 station.

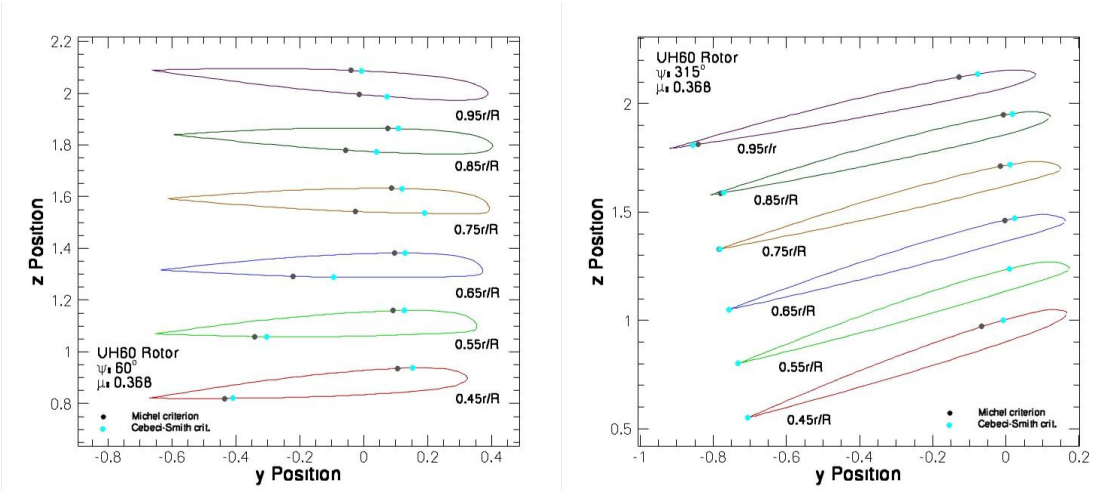

Figure 4: Transition onset for different sections of the UH-60A rotor. Results are for Michel's criterion and the Cebeci-Smith method. Two different azimuth angles were selected, at a=60º and a=315º. (μ=0.368 and M_{tip}=0.67).

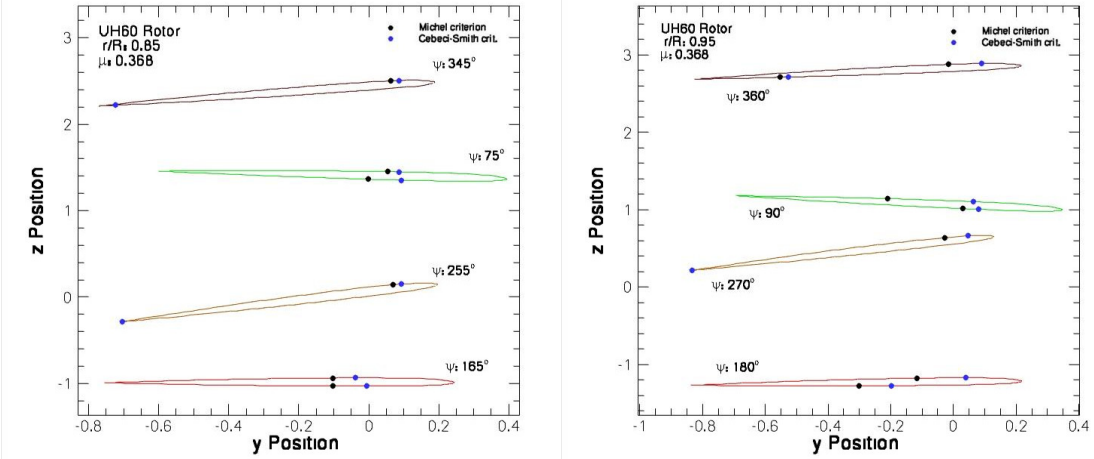

Figure 5: Transition onset for different azimuth of the UH-60A rotor. Results are for Michel's criterion and the Cebeci-Smith method. Two different stations were selected, at r/R=0.85 and r/R=0.95 (μ=0.368 and M_{tip}=0.67).

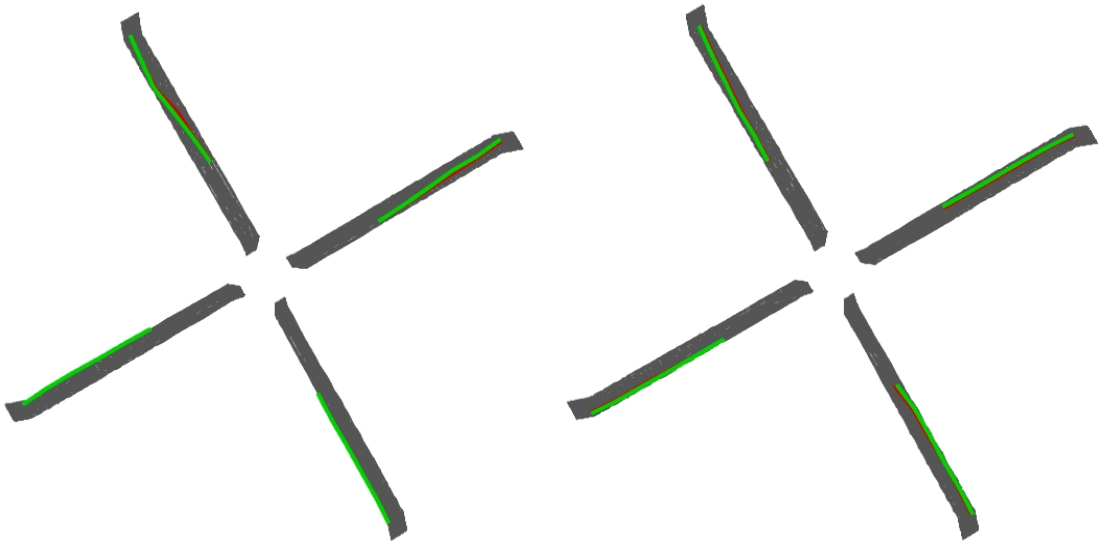

Figure 6: Transition onset boundary for a range of blade azimuth angles for the lower and upper surface of the UH-60A rotor. Results are shown for Michel's criterion and the Cebeci-Smith method ($a=30^o$-120^o-210^o-300^o, $\mu=0.368$ and $M_{tip}=0.67$).

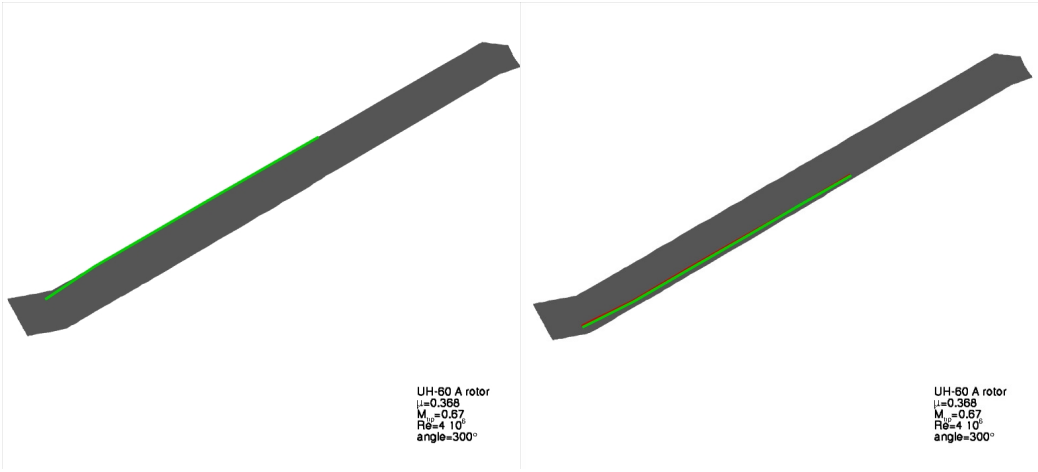

Figure 7: Detailed view of the lower and upper surface of the first blade for a UH-60A rotor where the transition onset is indicated. Results are shown for Michel's criterion and the Cebeci-Smith method ($a=300^o$, $\mu=0.368$ and $M_{tip}=0.67$).

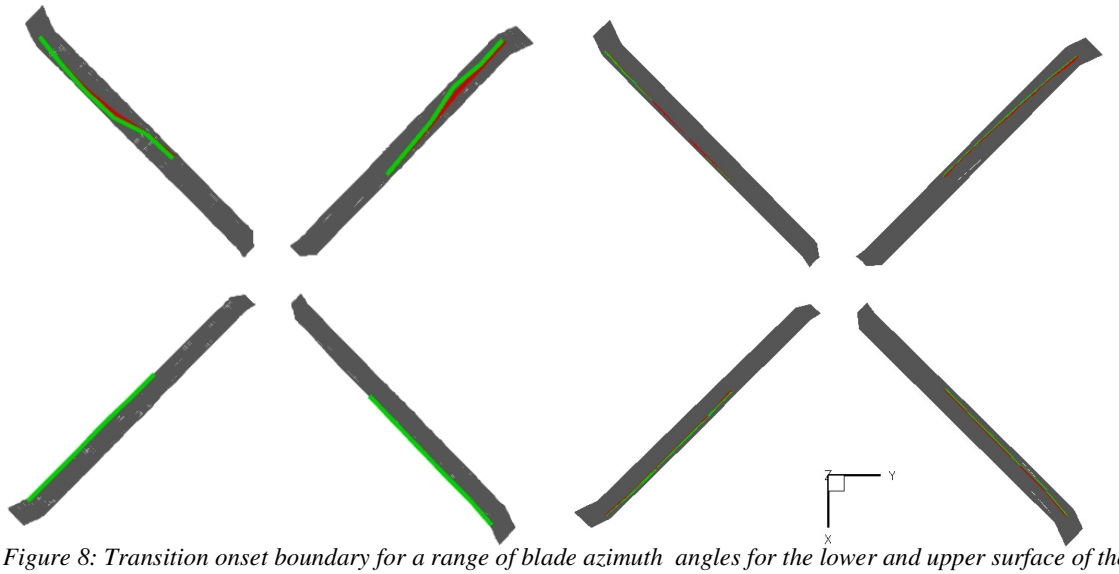

Figure 8: Transition onset boundary for a range of blade azimuth angles for the lower and upper surface of the UH-60A rotor. Results are shown for Michel's criterion and the Cebeci-Smith method. ($a=45^o$-135^o-225^o-315^o, $\mu=0.368$ and $M_{tip}=0.67$)

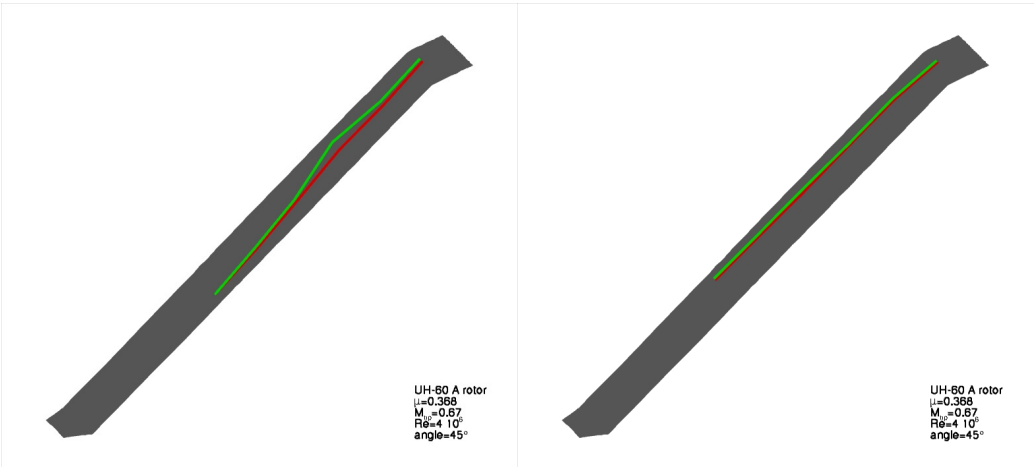

Figure 9: Detailed view of the lower and upper surface of the first blade for a UH-60A rotor where the transition onset is indicated. Results are shown for Michel's criterion and the Cebeci-Smith method ($a=45^o$, $\mu=0.368$ and $M_{tip}=0.67$).

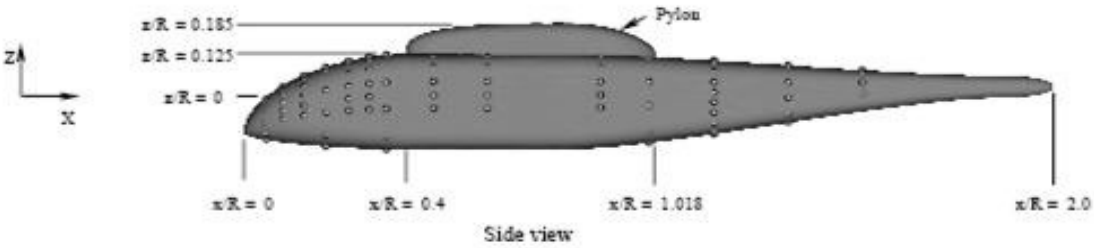

(a) Location of the pressure taps around ROBIN fuselage body.

Continued over

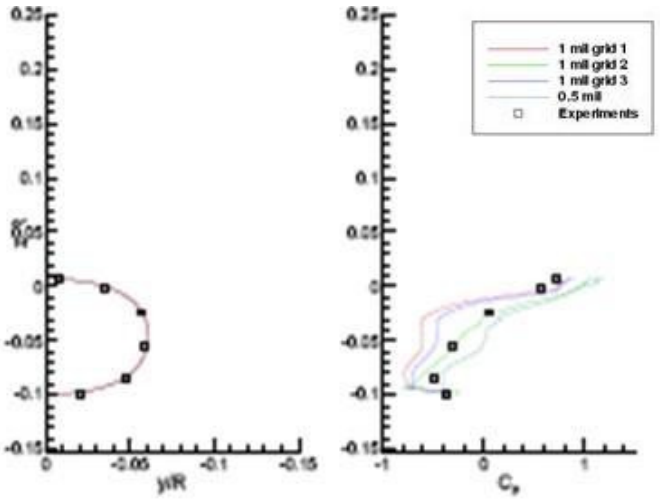

(b) x/R=0.0517

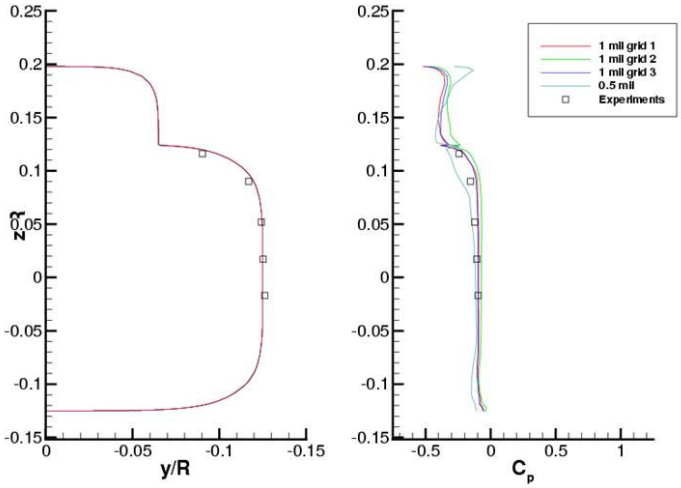

(c) x/R=0.6

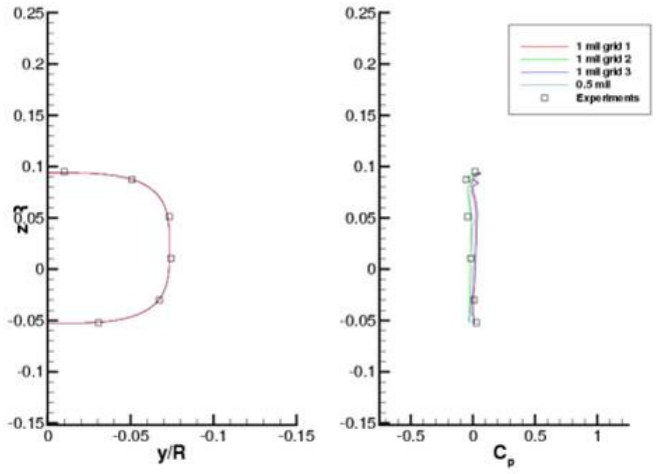

(d) x/R=1.345

Figure 10: Comparison of experimental and computational surface pressure distributions at different stations along the ROBIN fuselage. Results for three grid topologies are shown (a=5°, M=0.064 and Re=4.47 10^{6}).

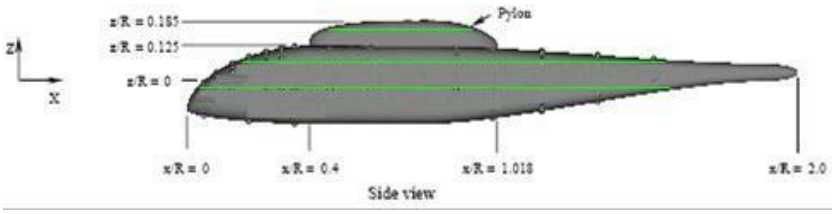

Schematic of the geometry of the ROBIN fuselage body.

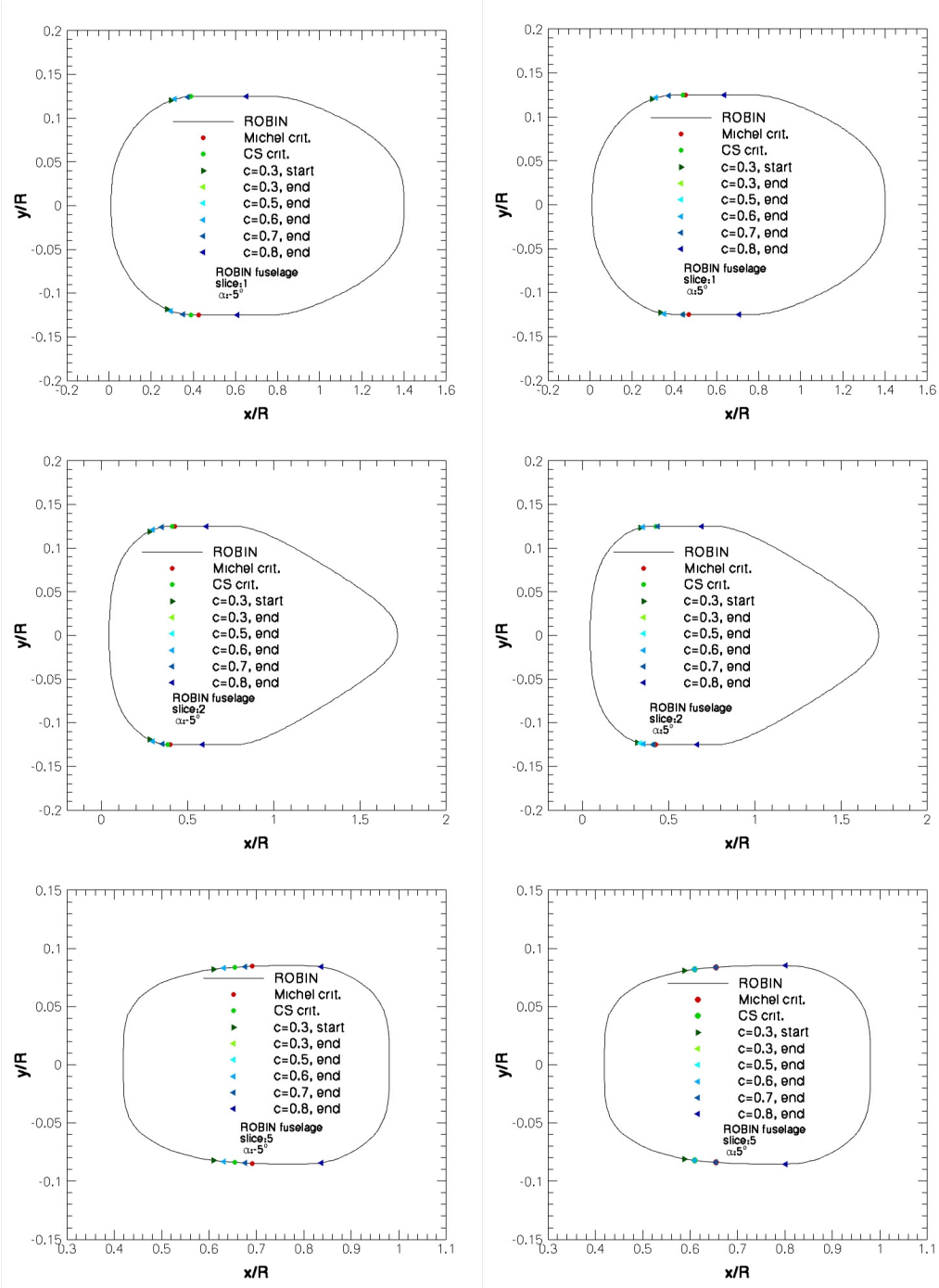

Figure 11: Transition onset for three different slides over the ROBIN fuselage. Results are for Michel criterion, Cebeci-Smith method and Abu-Ghannam and Shaw method. Two different angles of attack were selected at a=-5^o and a=5^o. (M=0.064 and Re=4.47 10^6)

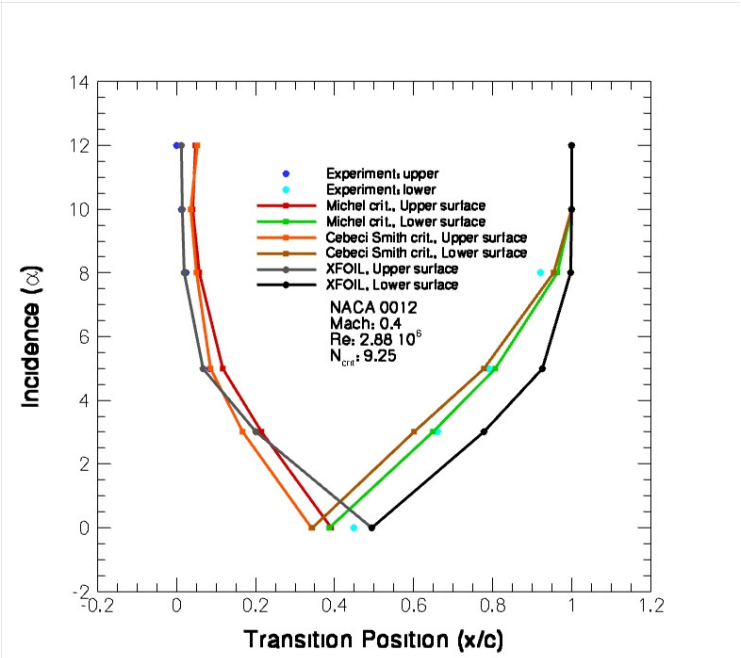

Figure 12: Location of transition onset for a NACA 0012 aerofoil as function of incidence angle. Comparisons are shown for Michel's criterion and the Cebeci-Smith method (Mach=0.4, Re=2.88 10^6 and N_{crit}=9.25).

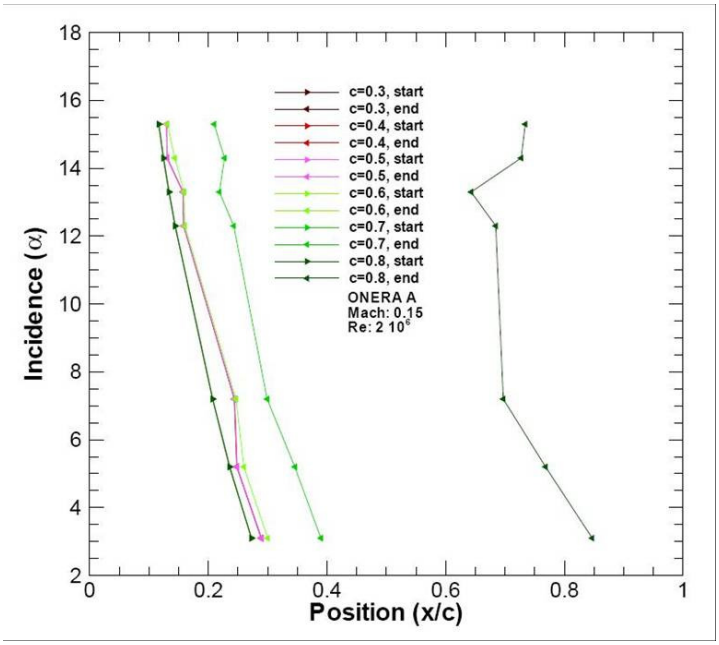

Figure 13: Onset and end of transition over a NACA 0012 aerofoil as a function of the incidence angle. The results are based on the Abu-Ghannam and Shaw model (Mach=0.2, Re=10^5 and N_{crit}=11.05).

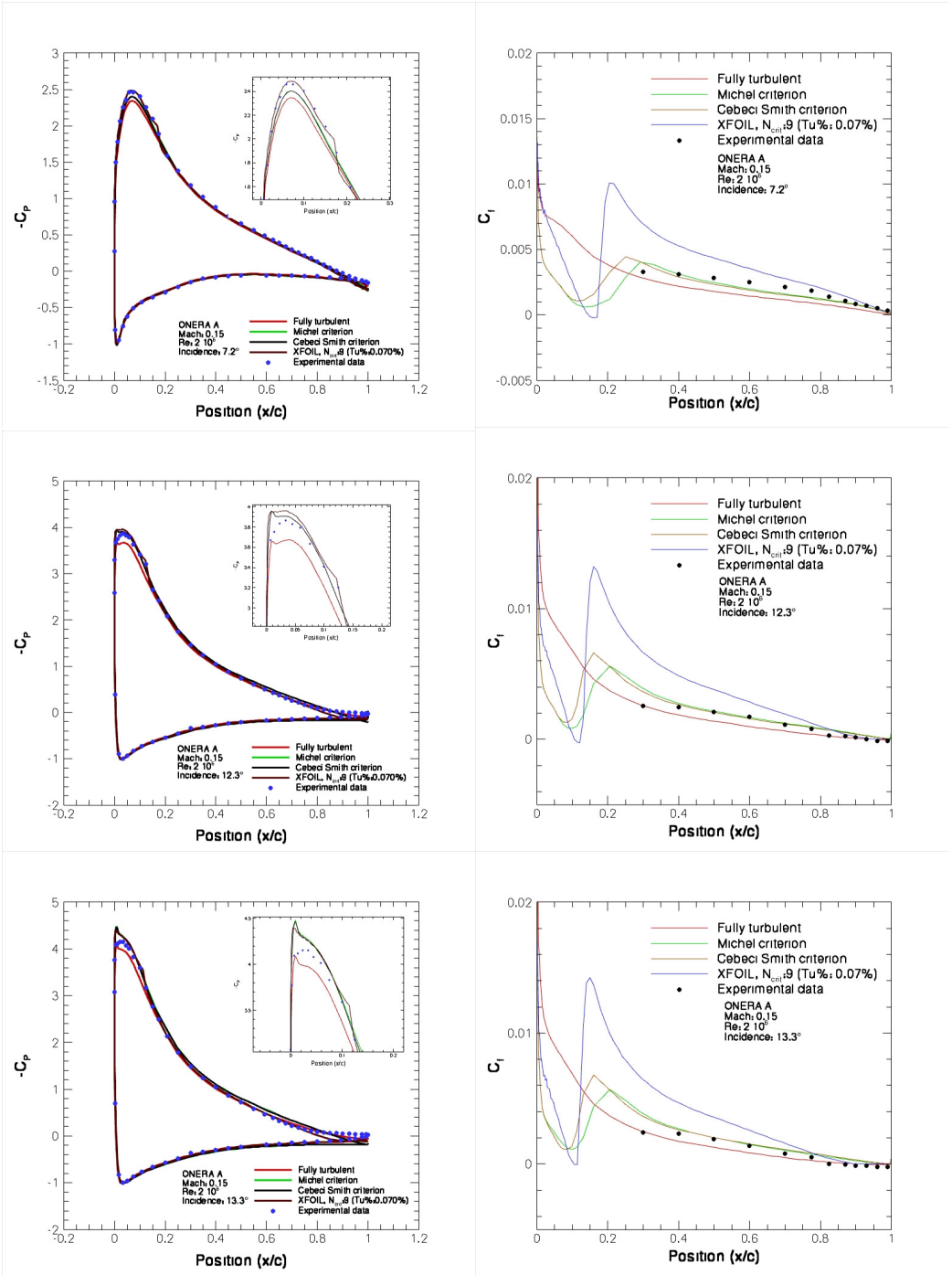

Figure 14: Surface pressure and skin friction coefficients over an ONERA A-Aerofoil. Experimental data from the F2 tunnel of ONERA are compared against fully turbulent calculations, Michel's criterion, Cebeci-Smith method and calculations using the XFOIL code. Three different incidence angles have been considered at a=7.2^o, 12.3^o and 13.3^o (Mach=0.15, Re=2 10^6 and N_{crit}=9).

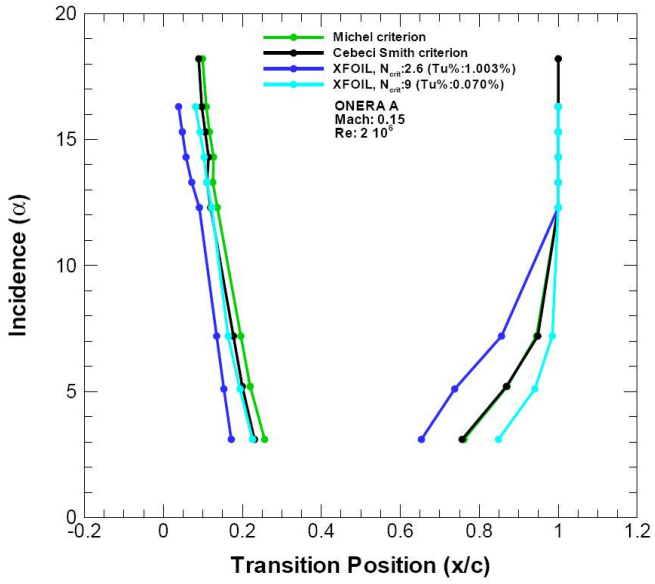

Figure 15: Location of transition onset on an ONERA A-Aerofoil as function of the incidence angle. Predictions are presented for Michel's criterion, the Cebeci-Smith method and calculations from XFOIL code. XFOIL results are shown for two critical values, N_{crit}=2.6 and N_{crit}=9. (Mach=0.15 and Re=2 10^6).

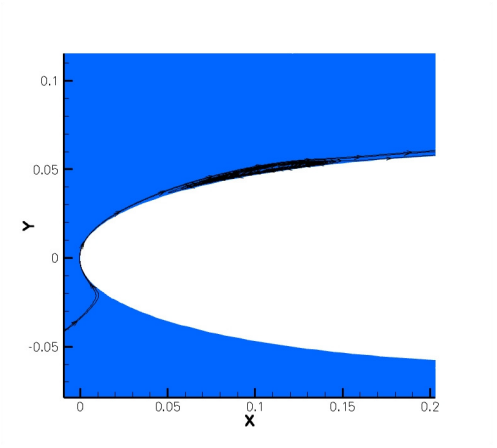

(a) γ-field

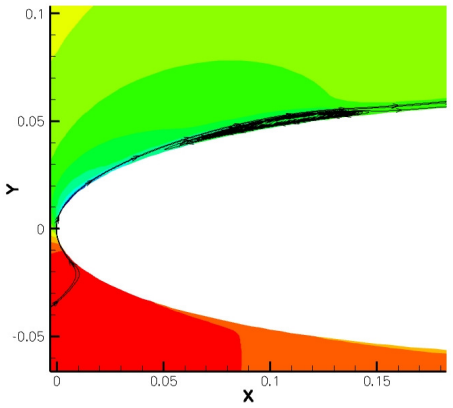

(b) Pressure-field

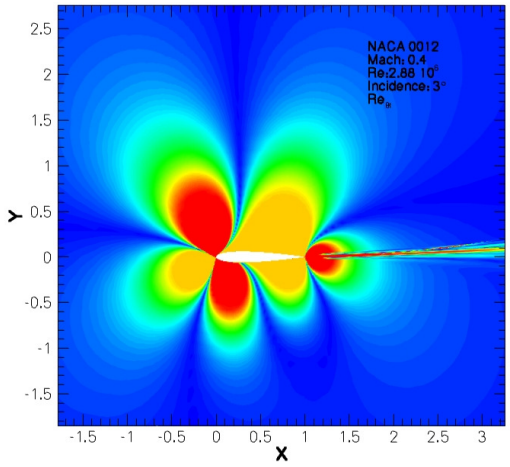

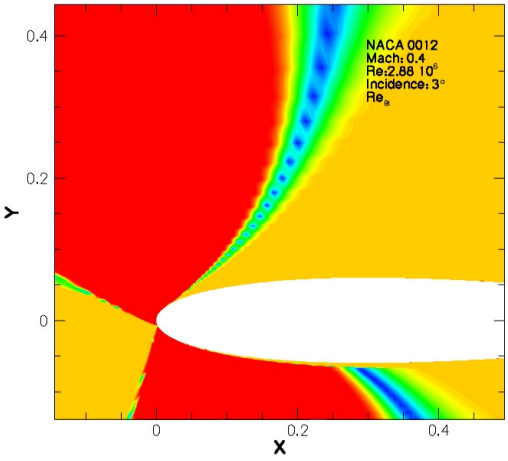

(c,d) Blending function for estimation of local Re_θ (full domain and detailed view)

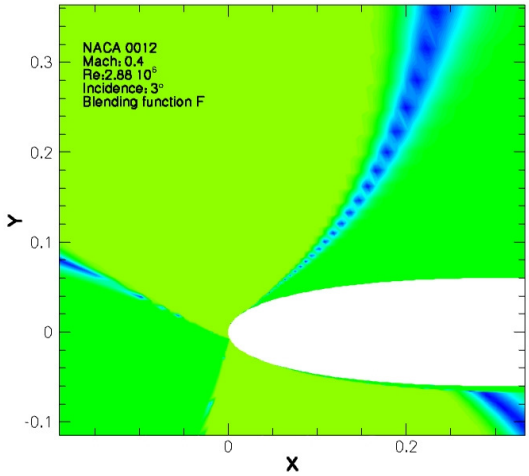

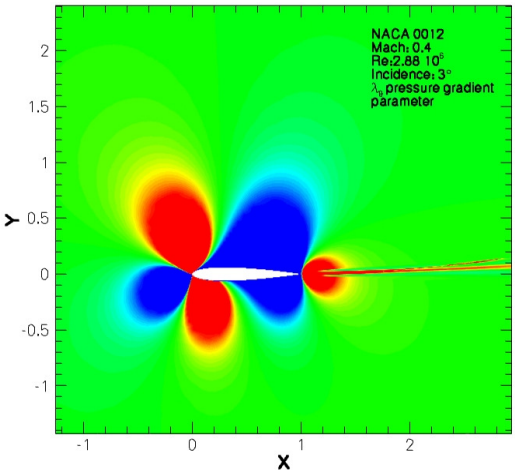

(e) Flow Acceleration Parameter *(f) Pressure Gradient Parameter*

Figure 16. Flow visualization of parameters and functions of the κ-ω-γ-Re_θ transition model. NACA 0012 aerofoil ($a=3^o$, Mach=0.4, $Re=2.88\ 10^6$).